Biasing the Screw-Sense of Supramolecular Coassemblies Featuring Multiple Helical States

Nathan van Zee, M. F. J. Mabesoone, Beatrice Adelizzi, Anja R. A. Palmans, E. W. Meijer

Biasing the screw-sense of supramolecular co-assemblies featuring multiple helical states

Nathan J. Van Zee,[1,2*] Mathijs F. J. Mabesoone,[1] Beatrice Adelizzi,[1†] Anja R. A. Palmans,[1] E. W. Meijer[1*]

[1]Institute for Complex Molecular Systems and Laboratory of Macromolecular and Organic Chemistry, Eindhoven University of Technology, 5600 MB Eindhoven, The Netherlands. [2]Chimie Moléculaire, Macromoléculaire, Matériaux, ESPCI Paris, Université PSL, CNRS, 75005 Paris, France.

KEYWORDS: supramolecular chemistry, copolymerization, co-assembly, sergeants-and-soldiers, hydrogen bonding.

ABSTRACT: By enchaining a small fraction of chiral monomer units, the helical sense of a dynamic polymer constructed from achiral monomer units can be disproportionately biased. This phenomenon, known as the sergeants-and-soldiers (S&S) effect, has been found to be widely applicable to dynamic covalent and supramolecular polymers. However, it has not been exemplified with a supramolecular polymer that features multiple helical states. Herein, we demonstrate the S&S effect in the context of the temperature-controlled supramolecular copolymerization of chiral and achiral biphenyl tetracarboxamides in alkanes. The one-dimensional helical structures presented in this study are unique because they exhibit three distinct helical states, two of which are triggered by co-assembling with monomeric water that is co-dissolved in the solvent. The self-assembly pathways are rationalized using a combination of mathematical fitting and simulations with a thermodynamic mass-balance model. We observe an unprecedented case of an "abnormal" S&S effect by changing the side chains of the achiral soldier. Although the molecular structure of these aggregates remains elusive, the co-assembly of water is found to have a profound impact on the helical excess.

INTRODUCTION

The handedness of a helical macromolecule is intricately tied to the structure of its constituent monomer units. Understanding this relationship is important not only for developing design principles of functional macromolecular systems but also for gaining insight into the origin of homochirality in Nature.[1] Early model studies aimed to elucidate the subtleties of this relationship were conducted on polyisocyanates, a well-studied class of helical covalent polymers.[2] Polyisocyantes are equally likely to adopt either a *P*- or *M*-helical structure when prepared from achiral isocyanates, but those synthesized from chiral analogues exhibit a preferred helical sense dictated by the absolute configuration of the monomer unit. In 1989, Green and co-workers[3] reported that copolymers of an achiral isocyanate with a small fraction of a chiral isocyanate exhibit a disproportionate helical bias. This phenomenon is called the sergeants-and-soldiers (S&S) effect,[4-6] and numerous subsequent studies have shown that it is applicable to both covalent[7-17] and supramolecular[18-28] polymers.

To quantify the degree of helical bias, it is necessary to have a clear understanding of the polymer composition to allow for the fraction of chiral monomer units to be unambiguously correlated to the net helicity. In the case of covalent helical copolymers, well-defined compositions are readily accessed via controlled polymerization protocols, and numerous analytical techniques are routinely available to confirm the structure after synthesis. These considerations are especially useful in understanding the S&S effect in systems that feature multiple helical states. Suginome and co-workers[29-31], for example, showed that certain homochiral poly(quinoxaline-2,3-diyl)s form helices of one sense in chloroform and helices of the opposite sense in 1,1,2-trichloroethane. They discovered that the transition is a result of the solvent-dependent extension and contraction of the side chains along the polymer backbone.[32] Copolymers of achiral and chiral units exhibit strong helical bias that can be predicted based on the absolute configuration of the chiral monomer, the copolymer composition, and the solvent composition.[31] Intriguingly, certain copolymers with a low sergeant fraction exhibit an "abnormal" S&S effect, in which a chiral unit exhibits one helical sense in a homopolymer and the opposite helical sense in a copolymer with achiral units.[11,33-41]

In stark contrast, the composition of supramolecular helical copolymers is challenging to characterize because

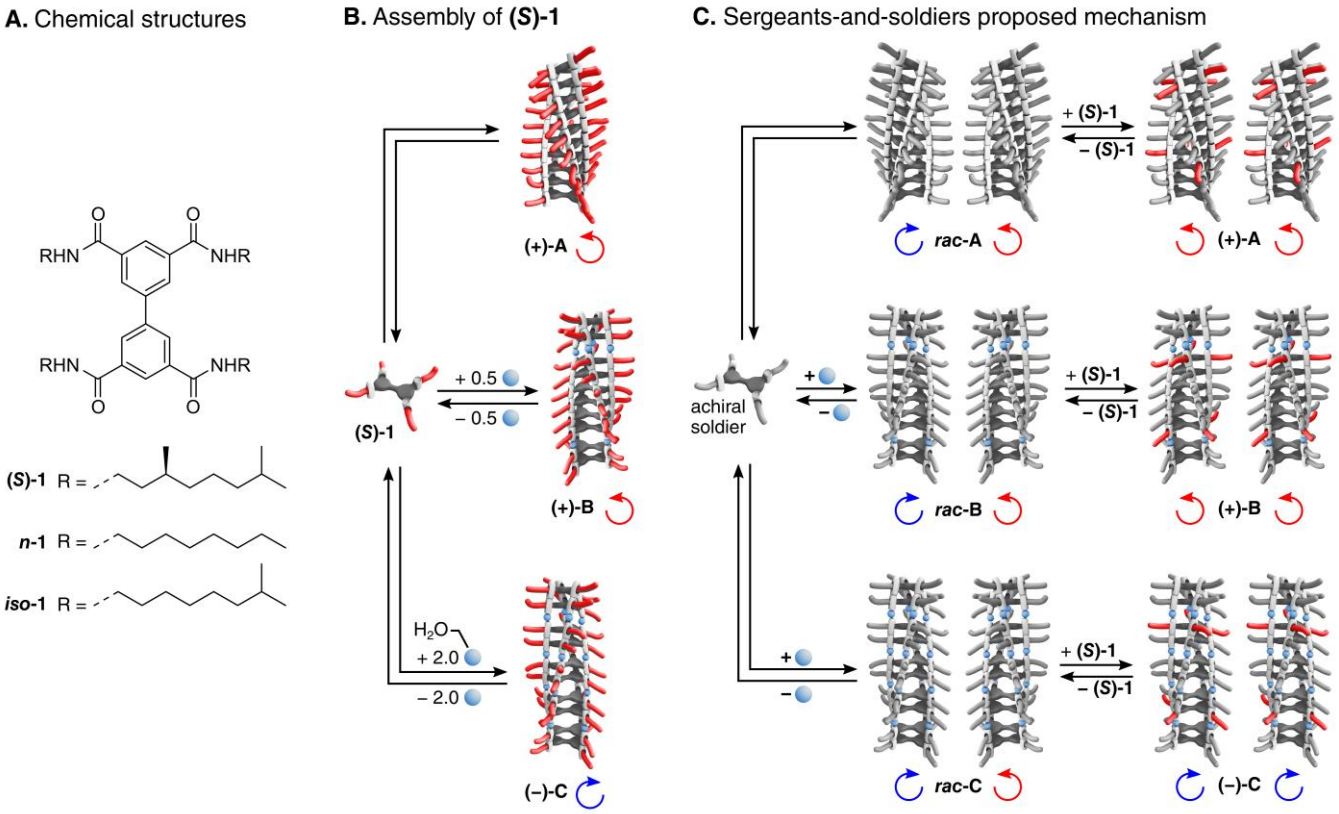

Figure 1. (A) Chemical structures of biphenyl tetracarboxamides **1**. (B) Schematic mechanism for the assembly of **(*S*)-1** (red units) in the presence of co-dissolved water (blue spheres, stoichiometries are given relative to 1 equiv. **(*S*)-1** monomer). (C) Proposed mechanism for the assembly of achiral biphenyl tetracarboxamides (grey units) with water (blue spheres) into racemic aggregates (middle structures) Incorporation of **(*S*)-1** (red units) biases the helicity of each respective aggregate.

of the dynamic, non-covalent nature of the interactions that hold the monomer units together. Supramolecular copolymers generally do not terminate, and thus they feature a fluxional composition that responds to changes in environmental conditions, such as temperature, solvent, and light. For some supramolecular copolymers, kinetic traps[26,42] and pathway complexity[43] cause a given set of monomers to form multiple kinds of aggregates depending on the conditions of synthesis. Such complexity demands that multiple experimental and theoretical techniques be combined to generate a comprehensive picture of the supramolecular structure.[44]

It is in this context that our group became intrigued by the supramolecular co-assembly of enantiopure biphenyl tetracarboxamide **(*S*)-1** (Figure 1A) and water molecules.[45] At micromolar concentrations in methylcyclohexane (MCH), **(*S*)-1** supramolecularly polymerizes via a nucleation-elongation mechanism into helical one-dimensional fibers assigned as (+)-**A**, which has a positive Cotton effect at 258 nm by circular dichroism (CD) spectroscopy. Depending on the temperature and concentration of co-dissolved water, (+)-**A** undergoes sharp transitions to form two other kinds of aggregates, (+)-**B** and (–)-**C**, that exhibit distinct helicities. The aggregate (+)-**B** has a positive Cotton effect at 250 nm, and (–)-**C** has a negative Cotton effect at 238 nm. Based on spectroscopic, calorimetric, and light scattering measurements, (+)-**B** and (–)-**C** form as a result of the co-assembly of **(*S*)-1** with water molecules under thermodynamic control. Using a modified version of the thermodynamic mass-balance model developed by ten Eikelder and Markvoort,[46] the stoichiometry of (+)-**B** and (–)-**C** was estimated to be 0.5 and 2.0 molecules of water per molecule of **(*S*)-1**, respectively (Figure 1B).

We envisioned that the chiral monomer **(*S*)-1** could act as a sergeant in S&S experiments, directing the helicity of supramolecular copolymers with achiral biphenyl tetracarboxamides in concert with co-dissolved water as schematically represented in Figure 1C. In this framework, the helical state is putatively controlled by a balance of the following parameters: the temperature; the total concentration of biphenyl tetracarboxamide; the water content; and the ratio between the chiral sergeant **(*S*)-1** and the achiral soldier. To the best of our knowledge, the S&S effect has not yet been demonstrated with a supramolecular copolymer featuring multiple helical states. Moreover, determining the composition of the system as a function of temperature presents a formidable challenge in calculating the net helicity for each state.

Herein, we demonstrate the S&S effect in this system and qualitatively deconvolute the temperature-dependent, multi-state behavior using a combination of mathematical fitting and simulations of spectroscopic data using an expanded version of the mass-balance mod-

el.[46] This approach allows us to rationally calculate net helicities and compare the degree of helical bias as a function of composition. Interestingly, introducing a small structural change to the achiral soldier gives rise to an "abnormal" S&S effect in one of the helical states, representing the first example of this effect for a supramolecular copolymer. Finally, the co-assembly of water is found to play a profound role in dictating the strength and selectivity of the helical bias induced by the chiral sergeant.

RESULTS AND DISCUSSION

Evaluation of *n*-1 as an achiral soldier. In line with our previous S&S studies,[47] *n*-octylcarboxamide groups were initially chosen as achiral side chains for the biphenyl tetracarboxamide soldier ***n*-1** (Figure 1A). The bulk properties of ***n*-1,** characterized by Fourier transform infrared spectroscopy (FTIR), differential scanning calorimetry (DSC), and polarized optical microscopy (POM; Figures S1, S2A, and S3, respectively), resemble those of **(*S*)-1** in the bulk.[45] In the course of preparing samples for spectroscopic studies in solution, we found that ***n*-1** is poorly soluble in MCH and other lower alkanes even with vigorous heating, stirring, and sonication. Surprisingly, the addition of 1 mol% of **(*S*)-1** to suspensions of ***n*-1** in MCH permits the formation of homogeneous solutions, which qualitatively indicates that these molecules interact with each other. In attempts to visualize aggregates formed under these conditions by atomic force microscopy (AFM), only large amorphous deposits were observed (Figure S5A and S5B). We suspect that the fibers collapse upon depositing onto the substrate surface.

We proceeded to study ***n*-1** with 1 mol% **(*S*)-1** with a total concentration of 30 μM in MCH by variable temperature (VT) CD and UV spectroscopy (Figure 2A and 2B). Spectra were acquired at 2 °C intervals as the sample was cooled from 95 to 5 °C, and the sample was equilibrated for 5 minutes prior to each measurement. The UV absorbance maximum hypsochromically shifts from 225 nm to less than 215 nm as the temperature is decreased (Figure 2A, bottom left). Following the UV absorbance maximum at 225 nm (Figure 2B, solid red triangles), the signal intensity non-sigmoidally decreases between 95 and 49 °C, indicating a cooperative supramolecular polymerization. However, the absence of a plateau before this transition suggests that the elongation temperature for this initial species is above 95 °C at this concentration. The corresponding CD spectra within this temperature range show only a modest helical bias (Figure 2A, left top, and Figure 2B, solid blue circles). Cooling between 49 and 21 °C initiates a transition to another species based on UV absorbance (Figure 2A, center bottom, and Figure 2B, solid red triangles). The low intensity of the CD signal exhibited between 95 and 21 °C prevents structural assignment (Figure 2A, center top). However, cooling below 21 °C results in a sharp transition evident in both the CD and UV channels (Figure 2A, right). The CD spectrum of this final species matches that of **(–)-C**, although comparing the intensity of the signal to that of to 100 mol% **(*S*)-1** at the same concentration (Figure 2B, open blue circles) suggests incomplete biasing of the helical sense.

The formation of **(–)-C** at low temperature even with only 1 mol% **(*S*)-1** is promising preliminary evidence that **(*S*)-1** and ***n*-1** act as a sergeant and soldier, respectively. This point can be further illuminated by comparing the intensity of the CD effect in each state as a function of sergeant content, which is most conveniently discussed in terms of net helicity (i.e., the ratio of the CD signal of the S&S copolymer to that of the enantiopure homopolymer in a given state). Reflecting upon previous S&S studies,[47] an important consideration is that temperature can strongly influence net helicity. Furthermore, the calculation of net helicity assumes that the monomers are fully assembled and that they form a mixture of *P*- and *M*-helices of a single state—thus, understanding the population of each state as a function of temperature is also essential.

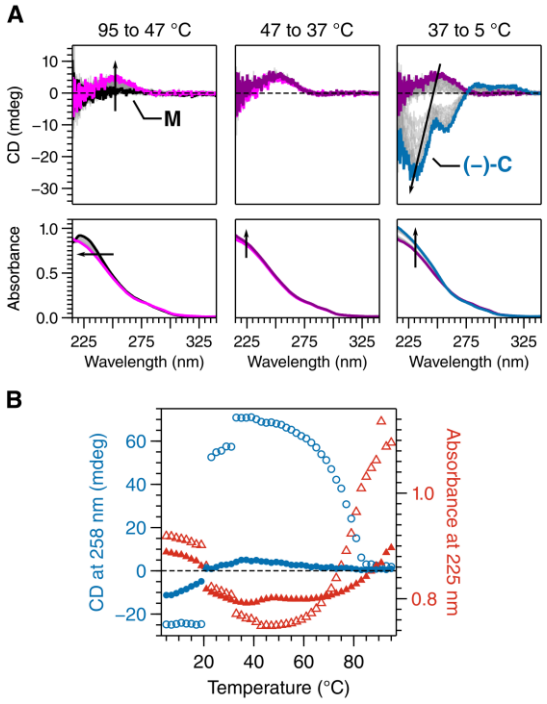

Figure 2. (A) CD (top) and UV (bottom) spectra of ***n*-1** with 1 mol% **(*S*)-1** and a total concentration of 30 μM in MCH. Water content was measured to be 31 ± 2 ppm. Spectra were acquired in 2 °C intervals as the sample was cooled between 95 and 5 °C. Arrows indicate spectra changes within the indicated temperature window. (B) Comparison of traces of CD at 258 nm (blue circles) and UV absorption at 225 nm (red triangles) for ***n*-1** with 1 mol% **(*S*)-1** (solid symbols) and 100 mol% **(*S*)-1** (open symbols).

These issues are addressed in the subsequent sections using a combination of experiments and theoretical modelling. To gain insight into the relationship between temperature and the net helicity within different states, the concentration of co-dissolved water is modulated to shift the transition temperatures. These data are then fitted or simulated using a thermodynamic mass-balance model to provide insight into the speciation of the S&S experiments

as a function of temperature. These analyses allow net helicities for each state to be rationally calculated and compared.

Co-assembly of soldier *n*-1 with sergeant (*S*)-1 under dry conditions. The transition temperatures of (+)-**A**→(+)-**B** and (+)-**B**→(–)-**C** for the homopolymer of (***S***)-**1** depend on the concentration of water.[45] Similar behavior was predicted for the co-assembly of ***n*-1** and (***S***)-**1**. A series of samples with 40, 60, 75, 90 and 100 mol% (***S***)-**1** (total concentration of 30 μM) was thus prepared and dried in a desiccator charged with phosphorus pentoxide (see Figure S6A). These samples contained 20 ± 2 ppm water based on Karl-Fischer titration. They were then analysed by VT-CD and -UV spectroscopy using the same protocol as described above (see Figures S7–S12). The CD (top, circles) and UV (bottom) traces in Figure 3 show that the transitions of (+)-**A**→(+)-**B** and (+)-**B**→(–)-**C** are shifted to lower temperatures compared to those observed for the experiment displayed in Figure 2, which was performed under ambient conditions. Decreasing the concentration of water effectively pushes these transitions outside the temperature window in this experiment. The CD and UV traces both show that the elongation temperature of **M**→(+)-**A** slightly increases as the fraction of (***S***)-**1** is increased based on both the CD and UV traces. The intensity of the CD signal is diminished as the fraction of (***S***)-**1** is decreased—this is particularly evident at temperatures below 70 °C.

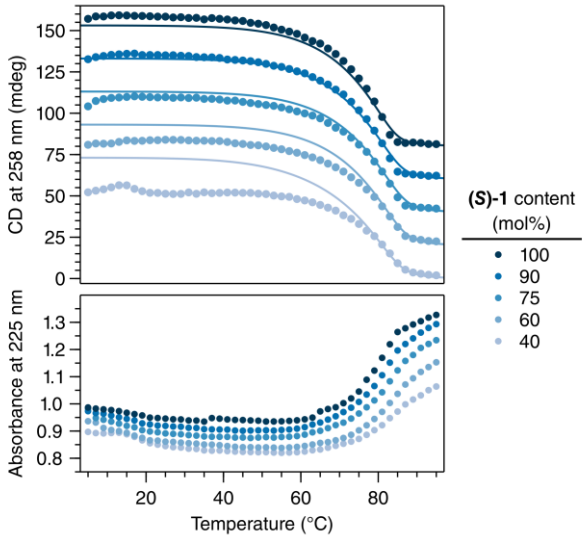

Figure 3. Variable temperature (VT) CD (top) and UV absorbance (bottom) experiments with varying amounts of sergeant (***S***)-**1** and a water concentration of 20 ± 2 ppm. In the plot of CD data, the solid line corresponds to the fit using the thermodynamic mass-balance model. For clarity, each experimental CD curve and corresponding fit are vertically offset by increments of 20 mdeg.

The thermodynamic mass-balance model for supramolecular copolymerizations recently reported by ten Eikelder and colleagues[48] was used to gain further insight into the nature of the initial co-assembly of (***S***)-**1** and ***n*-1**. We specifically aimed to fit the experimental CD data in the region of the **M**→(+)-**A** transition to calculate the enthalpy of the hetero-interaction between (***S***)-**1** and ***n*-1**, which is critical for developing a reasonable simulation of the entire system (*vida infra*). Accurate thermodynamic parameters for the homopolymerization of (***S***)-**1** are required. Thus, as a preliminary step, the previously-reported VT-CD data[45] were fitted using this model (see Figure S36 and associated discussion in the Supporting Information).

Several challenges in this system required the simplification of assumptions to make the fits feasible. Because of the insolubility of ***n*-1** in MCH (*vide supra*), it was not possible to experimentally determine the thermodynamic parameters for the homopolymerization of ***n*-1**. We therefore estimated based on the VT-UV data presented in Figure 2B that the elongation temperature of 30 μM solutions of ***n*-1** is 108 °C, corresponding to an enthalpy of elongation of –92 kJ mol^{-1}. Additionally, since the mass-balance models for supramolecular copolymerizations are computationally intensive, the number of fit parameters had to be minimized. The entropy of elongation and the nucleation penalty of the copolymerization of (***S***)-**1** and ***n*-1** were assumed to be equal to those of the homopolymerization of (***S***)-**1**, and the hetero-interaction between (***S***)-**1** and ***n*-1** were assumed to be symmetric with the hetero-interaction of ***n*-1** and (***S***)-**1**. These assumptions are in line with those made in previous uses of this model.[49-50]

The resulting fits of the CD data are represented as solid lines in Figure 3 (top). The CD effect and elongation temperatures of samples containing 75 mol% or more (***S***)-**1** is accurately fitted, but the helical bias of the samples containing 40 and 60 mol% (***S***)-**1** is overestimated. The mismatch penalty (i.e., the energetic penalty for (***S***)-**1** to aggregate into polymers of disfavored helicity) could thus not be determined accurately (Figure S37). Nevertheless, the model accurately describes the elongation temperatures of all mixtures, which directly correspond to the enthalpies of the homo- and hetero-interactions.[48] We calculated the enthalpy of the hetero-interaction between (***S***)-**1** and ***n*-1** of –83 kJ mol^{-1}, which is slightly different than that of the homo-interactions of (***S***)-**1** (ΔH_e= –86 kJ mol^{-1}), agreeing with observations for similar systems.[49-52]

Co-assembly of soldier *n*-1 with sergeant (*S*)-1 under wet conditions. The transition temperatures of (+)-**A**→(+)-**B** and (+)-**B**→(–)-**C** are shifted back into the temperature window of interest by increasing the water content. Eleven mixtures of ***n*-1** and (***S***)-**1** with ratios ranging from 1 to 100 mol% in 10 mol% intervals were prepared, all with a total monomer concentration of 30 μM in MCH. To ensure that the samples contained approximately the same concentration of water, they were simultaneously conditioned in a humidifying chamber that was charged with brine and MCH (Figure S6B). Based on Karl Fischer titrations, these samples contained 31 ± 2 ppm of water. After conditioning, the samples were sealed and analyzed by VT-CD and -UV spectroscopy again using the same protocol described above.

To understand the complete data set, it is instructive to first evaluate the CD spectra of the aggregation of ***n*-1** with 60 mol% **(*S*)-1** (Figure 4A and 4B). The species at 95 °C designated as **M** exhibits no CD signal and a UV response that is similar to that observed for solutions of pure **(*S*)-1** at high temperature.[45] Upon cooling, the CD signal slightly increases until reaching 85 °C, below which the CD signal undergoes a non-sigmoidal increase in intensity. The resulting aggregate is characterized by a positive Cotton effect at 258 nm, consistent with the formation of (+)-**A**. Cooling further to 29 °C causes a sharp transition to a new species with a positive Cotton effect at 250 nm, matching the previously reported spectrum of (+)-**B**. Cooling below 19 °C results in a final species with a negative Cotton effect at 238 nm that matches the expected spectrum of (–)-**C**. This sequence of transitions closely matches the assembly pathway reported[45] for the homopolymerization of **(*S*)-1** and conforms to the predicted mechanism outlined in Figure 1C. An analogous set of CD spectra for all compositions along with corresponding UV spectra and cooling curves are presented in Figures S13-S21.

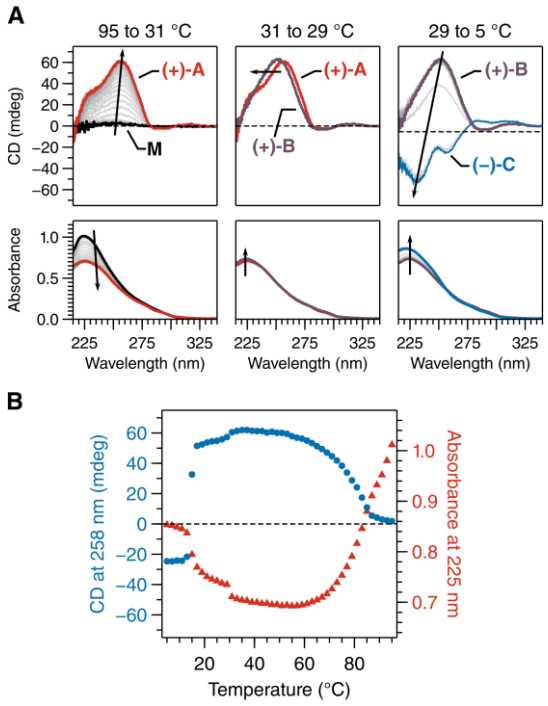

Figure 4. (A) CD (top) and UV (bottom) spectra of ***n*-1** with 60 mol% **(*S*)-1** and a total concentration of 30 μM in MCH. The water concentration is 31 ± 2 ppm. Spectra were acquired in 2 °C intervals as the sample was cooled between 95 and 5 °C. Arrows indicate spectra changes within the indicated temperature window. (B) Traces of CD at 258 nm (blue circles) and UV absorption at 225 nm (red triangles).

To facilitate making comparisons between the different compositions, the CD intensities at 258 nm across all temperatures and compositions are represented as a heat map (Figure 5B). A plot of annotated cooling curves of 100 mol% **(*S*)-1** and 60% **(*S*)-1** with 40% ***n*-1** is positioned above the heat plot to serve as a visual reference for the expected temperature ranges of (+)-**A**, (+)-**B**, and (–)-**C**. The aggregation pathway of compositions with at least 30 mol% **(*S*)-1** closely follows that of 100 mol% **(*S*)-1**. That is, the CD spectra of each state matches well with those of (+)-**A**, (+)-**B**, and (–)-**C** in the expected temperature ranges (Figures S14–S19). At **(*S*)-1** content below 30 mol%, the CD spectra in the temperature range expected for (+)-**A** do not match well with the reference spectrum for (+)-**A** (Figures S20 and S21), nor do they appear to be linear combinations of (+)-**A** and (+)-**B**. The helical structure of these co-assemblies thus is not the same as that of (+)-**A**.

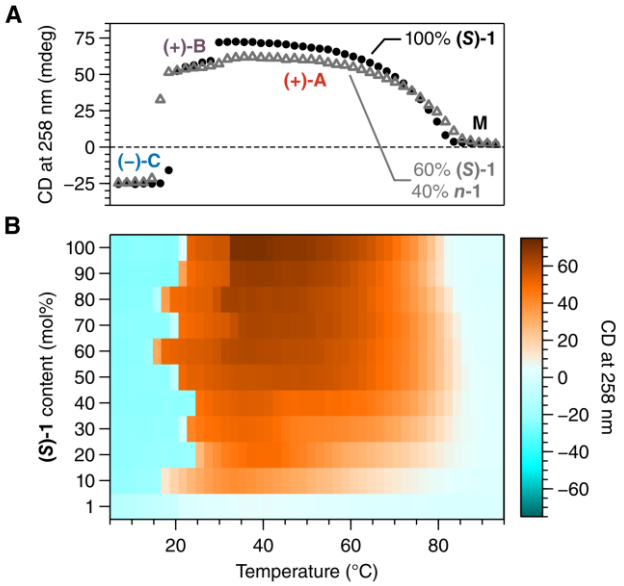

Figure 5. (A) Annotated CD cooling curves (top) for 30 μM samples of 100% **(*S*)-1** (black filled circles) and 60% **(*S*)-1** with 40% ***n*-1** (grey open triangles). (B) Heat plot of the CD intensity at 258 nm for S&S mixtures with ***n*-1** and **(*S*)-1** (**M** = molecularly dissolved monomers, $[H_2O]$ = 31 ± 2 ppm).

Based on CD, the transition temperature of **M**→(+)-**A** increases as the sergeant fraction is decreased from 100 to 50 mol%, reaching a maximum of about 87 °C. However, as the sergeant content is decreased from 50 to 1 mol% sergeant, the transition temperature decreases. Interestingly, the VT-UV measurements show that the **M**→(+)-**A** transition temperature consistently increases from 83 °C to above 95 °C as the **(*S*)-1** content is decreased from 100 to 1 mol%, contrasting to the behavior noted observed in the VT-CD traces. Most likely, aggregates formed at these high temperatures are rich in ***n*-1** with an insufficient fraction of copolymerized **(*S*)-1** to bias the helicity. In addition to a change in elongation temperature, across all compositions, the width of the transitions **M**→(+)-**A** and (+)-**A**→(+)-**B** increases, and the CD intensity of both (+)-**A** and (+)-**B** decreases as the sergeant content decreases. In contrast, the (+)-**B**→(–)-**C** transition is sharp at all composition ratios studied, and a strong CD effect for (–)-**C** is observed even at low sergeant fractions. The shape of the CD spectrum below approximately 20 °C is consistent with that of (–)-**C** across all compositions investigated (Figures S14-S21 and Figure 2A).

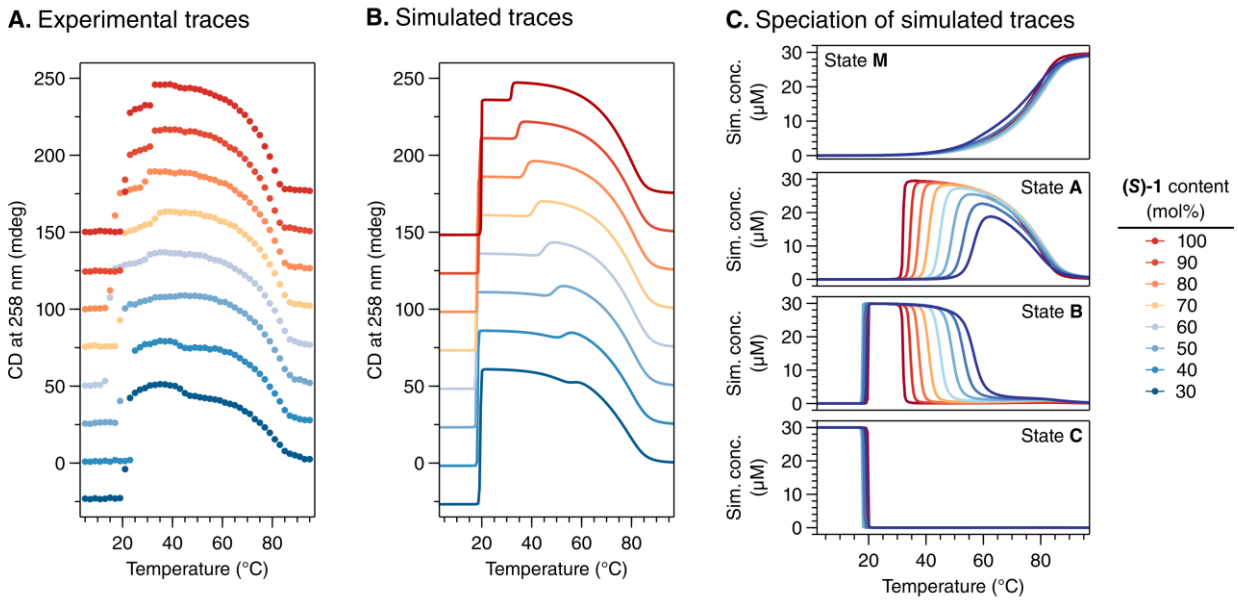

Figure 6. (A) Experimental CD traces of S&S mixtures with ***n*-1** and **(*S*)-1** (total [**1**] = 30 μM and [H_2O] = 31 ± 2 ppm water). The traces are vertically offset in increments of 25 mdeg for clarity. (B) Simulated CD traces of S&S mixtures with ***n*-1** and **(*S*)-1**. The traces are vertically offset in increments of 25 mdeg for clarity. (C) Speciation plots for each state observed in the simulated S&S experiments.

Simulation of sergeants-and-soldiers experiments. We attempted to fit the experiments presented in Figures 4 and 5 using the same routine that was applied to the experimental data presented in Figure 3. However, as a result of the experimental uncertainty in the water content measurements, no satisfactory fit could be obtained (see Supporting Information). Nonetheless, by simulating rather than fitting the data, several insights into this multicomponent assembly can be obtained. In these simulations, we start with the known thermodynamic parameters for **(*S*)-1** homo-interactions and the hetero-interaction for **(+)-A** determined above, and we made estimates for the unknown values for the homopolymerization of ***n*-1** and the other hetero-interactions. Both the enthalpies and entropies of the homo- and hetero-interactions of **(*S*)-1** and ***n*-1** in states **(+)-B** and **(–)-C** had to be independently selected (Table 1). With this set of parameters, we were able to obtain satisfactory reproduction of the experimental curves (Figure 6A and 6B). The only slightly less favorable hetero-interactions that were necessary to obtain the satisfactory reproduction suggest that the supramolecular copolymers all form 'blocky' structures, with alternating regions enriched in either monomer.[45,47]

The simulations closely follow the trends of the CD effect for all polymer states as well as the transition temperatures observed in the experimental data. For example, in the case of S&S experiments under both wet and dry conditions, the **(+)-A**→**(+)-B** transition broadens and the transition temperature increases as the sergeant content is decreased. This behavior is in contrast to the supramolecular homopolymerization of **(*S*)-1**, in which **(+)-A**→**(+)-B** is sharp and independent of the monomer concentration. To replicate this behavior in the simulations, ***n*-1** is assigned with thermodynamic parameters that are independent to those of **(*S*)-1**. The parameters of ***n*-1** were selected so that the free energies of **(+)-A** and **(+)-B** become closer together as the sergeant content is decreased. As can be seen in the simulated speciation plots (Figure 6C), the **(+)-B** state is populated at increasingly higher temperatures as the fraction of **(*S*)-1** sergeant is decreased. The formation of **(+)-A** and **(+)-B** is thus increasingly competitive as sergeant content is decreased, resulting in a wider temperature window in which these two aggregates co-exist. Indeed, we observe mixtures of **(+)-A** and **(+)-B** over broad temperature ranges in the experimental CD spectra presented in Figures S10–S11 and S16–S18.

In contrast, the **(+)-B**→**(–)-C** transition takes place over a narrow and constant temperature range across all compositions, and the transition temperature is essentially independent of the sergeant content. However, the transition temperature remains dependent on the water concentration regardless of the sergeant content. To realize this behavior in the simulations, the enthalpies and entropies of the homo- and hetero-interactions of **(*S*)-1** and ***n*-1** were set to be similar in value. An interesting feature of **(–)-C** is that its entropy of elongation is much more negative than those of **(+)-A** and **(+)-B**. We attribute this disparity to the incorporation of water molecules, as **(–)-C** contains more water in its structure than either **(+)-A** or **(+)-B**. The large entropic penalty gives rise to the characteristic dependence on water concentration observed in the formation of **(–)-C**.

One feature that is not well-captured in the simulation is the gradual decrease in the CD intensity of **(+)-B** as temperature is decreased. This behavior is observed both in the homopolymerization of **(*S*)-1** and in the co-

assembly of (***S***)-**1** and ***n***-**1**. A disparity in cooperativity is likely responsible for the putative co-existence of (–)-**C** with (+)-**B**. The fitting of the homopolymerization of (***S***)-**1** (see Supporting Information) indicates that the nucleation penalty for (+)-**B** is greater than that of (–)-**C**, suggesting that (+)-**B** is more cooperative than (–)-**C**.[48] The asymmetry of the (+)-**A**→(+)-**B** transition further supports this hypothesis.[53] The more isodesmic nature of (–)-**C** allows it to nucleate relatively easily and form with the small amount of free monomer that is not assembled into (+)-**B**; thus, (–)-**C** can co-exist with (+)-**B** even at a temperature at which (–)-**C** is less thermodynamically stable than (+)-**B**. Although the nucleation penalties were not optimized in the simulation to reflect this behavior, it is important to note the co-existence of (–)-**C** with (+)-**B** in considering net helicity calculations.

Table 1. Thermodynamic parameters used to simulate the S&S experiments.

Parameter	State A	State B	State C
$\Delta H_{e,\,(s)\text{-}1\text{—}(s)\text{-}1}$ (kJ·mol^{-1})	–86[a]	–101[a]	–131[a]
$\Delta S_{(s)\text{-}1\text{—}(s)\text{-}1}$ (J·mol^{-1}·K^{-1})	–155[b]	–167[c]	–204[c]
$\Delta H_{e,\,(s)\text{-}1\text{—}n\text{-}1}$ (kJ·mol^{-1})	–83[c]	–96[d]	–129[d]
$\Delta S_{(s)\text{-}1\text{—}n\text{-}1}$ (J·mol^{-1}·K^{-1})	–155[b]	–156[e]	–200[e]
$\Delta H_{e,\,n\text{-}1\text{—}n\text{-}1}$ (kJ·mol^{-1})	–92[d]	–100[d]	–134[d]
$\Delta S_{n\text{-}1\text{—}n\text{-}1}$ (J·mol^{-1}·K^{-1})	–155[d]	–145[d]	–198[d]
Mismatch penalty (kJ·mol^{-1})	85[c,f]	0.5[d]	0.2[d]

[a]Experimental value based on calorimetry and Van't Hoff analyses. [b]Value calculated using free energy relationships. [c]Value determined through fitting of experimental VT-CD curves using a thermodynamic mass-balance model. [d]Estimated values. [e]Calculated as the average of $\Delta S_{(S)\text{-}1\text{—}(S)\text{-}1}$ and $\Delta S_{n\text{-}1\text{—}n\text{-}1}$. [f]The mismatch penalty for state **A** could not be determined accurately, see Figure S37.

Calculation of net helicities. Based on the speciation plot (Figure 6C), over 97% of monomer is consumed at 45 °C, which allows for comparisons of net helicities to be made at and below this temperature. Based on the experiments in Figure 5, the transition temperature for (+)-**A**→(+)-**B** increases and the transition becomes broader as the sergeant content is decreased. In Figure 7, net helicities for (+)-**A** are plotted for experiments performed at 9, 19, and 45 °C under dry (red triangles) and wet (blue triangles) conditions. Since net helicities can only be reliably calculated when only a single polymer state is present, the net helicities with respect to the formation of (+)-**A** can only be calculated at temperatures and sergeant contents at which there is no co-existing (+)-**B**. For this reason, some points are excluded from this plot at low temperature and low sergeant content (see Supporting Information for details).

The bias of the screw-sense as a function of (***S***)-**1** content in (+)-**A** is not strong, exhibiting only modest amplification beyond a linear response. The net helicity is not strongly dependent on temperature between 9 and 45 °C, which contrasts with the temperature sensitivity reported for benzene tricarboxamides in S&S experiments.[47] The helical bias is also not strongly affected by changes in water concentration within this temperature range, which is expected because water is not a co-monomer for (+)-**A**.

The calculation of net helicities for (+)-**B** is complicated by three factors: the experimental uncertainty of the water content measurements; the broadening of the (+)-**A**→(+)-**B** transition with decreasing sergeant content; and the competition with the more isodesmic (–)-**C**. These factors preclude the quantitative comparison of the net helicities calculated for (+)-**B** with that observed in the other states. However, at sergeant fractions below 30 mol%, (+)-**B** is detected but (+)-**A** is not clearly detected (see Figures S20 and S21), which suggests that (***S***)-**1** is a stronger sergeant in (+)-**B** than in (+)-**A**.

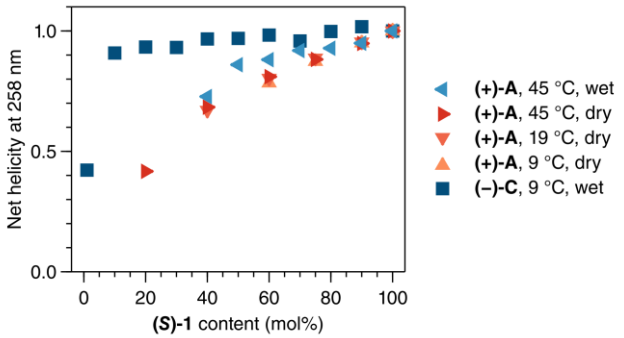

Figure 7. Comparison of net helicity as a function of (***S***)-**1** content for aggregates in states (+)-**A** and (–)-**C** at varying temperature and water content.

Most strikingly, strong biasing of the screw-sense is observed in the formation of (–)-**C** at low temperature (Figure 7, dark blue squares). Even at 1 mol% (***S***)-**1**, the co-assembly clearly forms (–)-**C**, as evidenced by the negative Cotton effect at 238 nm and the characteristic shoulder at 257 nm (Figure 2A), exhibiting a net helicity of 0.42. At 10 mol% (***S***)-**1**, the net helicity is over 0.90, and it approaches unity as the sergeant content is further increased. Using data sets for both wet and dry samples acquired at 9 °C, we can compare the net helicities of (+)-**A** and (–)-**C**. Although the net helicities for (+)-**A** cannot be calculated at low sergeant content (*vida supra*), at 60% (***S***)-**1** the net helicity observed for (–)-**C** is significantly higher than that of (+)-**A** (0.98 vs. 0.78, respectively). Since there is only a weak temperature dependence net helicities calculated for (+)-**A**, it is reasonable to compare the net helicities for (+)-**A** determined at higher temperatures with the net helicities of (–)-**C** acquired at 9 °C. At 20 mol% (***S***)-**1**, the net helicity for (–)-**C** at 9 °C is 0.93, while the net helicity for (+)-**A** at 45 °C is only 0.42. Although the molecular packing of these aggregates remains elusive, the co-assembled water molecules play a direct

role in amplifying the expression of the chiral sergeant within the helical aggregate.

Distal structural changes to the achiral soldier highlight subtle energy balances. In an attempt to address the poor solubility of ***n*-1**, we synthesized and studied an alternative achiral soldier, ***iso*-1**, that features four *iso*-nonylcarboxamide groups (Figure 1A). The bulk properties of ***iso*-1** were characterized by FTIR spectroscopy, DSC, and POM (Figures S1, S2B, and S4, respectively); its bulk properties are similar to those of ***n*-1** and **(*S*)-1**. Solutions of ***iso*-1** in MCH are readily prepared, and individual fibers with lengths on the order of microns were visualized by AFM (Figure S5C and S5D).

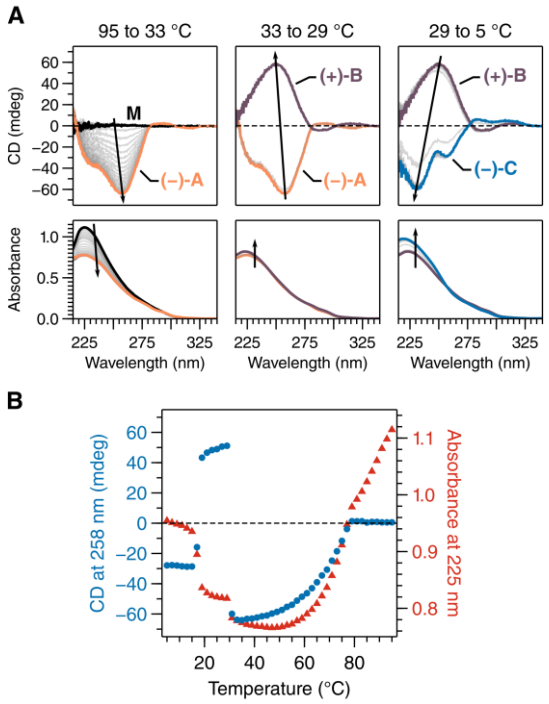

Figure 8. (A) CD (top) and UV (bottom) spectra of ***iso*-1** with 60 mol% **(*S*)-1** and a total concentration of 30 μM in MCH. The water concentration is 31 ± 2 ppm. Spectra were acquired in 2 °C intervals as the sample was cooled between 95 and 5 °C. Arrows indicate spectra changes within the indicated temperature window. (B) Traces of CD at 258 nm (blue circles) and UV absorption at 225 nm (red triangles).

A VT-CD and -UV study was performed using ***iso*-1** as the soldier and **(*S*)-1** as the sergeant under both wet and dry conditions (Figures S22–S35). In striking contrast to the results presented above using ***n*-1** as the soldier, the use of ***iso*-1** gives rise to an assembly pathway that does not conform to the mechanism presented in Figure 1C. We first consider in detail the S&S experiment with 40 mol% ***iso*-1** and 60 mol% **(*S*)-1** (Figure 8). Upon cooling below 79 °C, the monomers copolymerize to form a previously unobserved species that exhibits a negative Cotton effect at 258 nm and a UV spectrum that is nearly identical to that of (+)-**A**. In fact, the shape of the CD spectrum is the negative of that of (+)-**A** (Figure 3F), and thus this structure is assigned as (−)-**A**. Cooling below 33 °C results in the sharp transformation of (−)-**A** into (+)-**B**, and cooling below 17 °C results in the formation of (−)-**C**. The aggregate (−)-**A** is a thermodynamically stable structure and not a result of pathway complexity or kinetic traps because the temperature was equilibrated prior to each measurement. Additionally, (−)-**A** can be formed not only by cooling the solution from monomers but also by heating (+)-**B** above the (+)-**B**→(−)-**A** transition temperature.

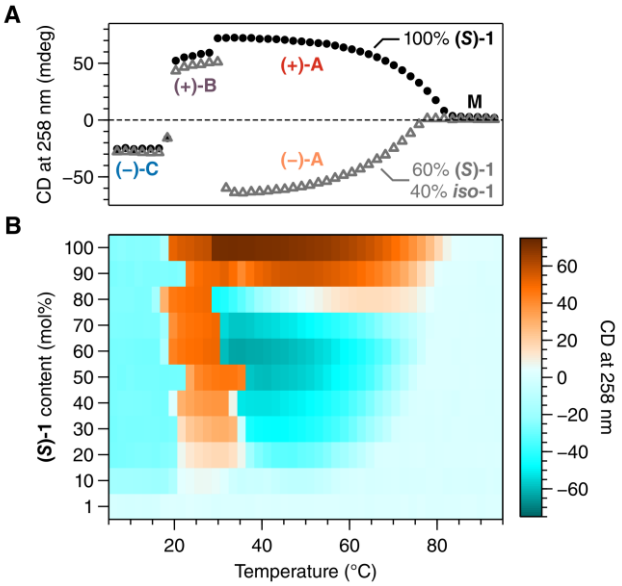

Figure 9. (A) Annotated CD cooling curves for 30 μM samples of 100% **(*S*)-1** (black solid circles) and 60% **(*S*)-1** with 40% ***iso*-1** (grey open triangles). (B) Heat plot of the CD intensity at 258 nm for S&S mixtures with ***iso*-1** and **(*S*)-1** ([H_2O] = 31 ± 2 ppm).

The full set of results of the VT-CD experiments under wet conditions are represented as a heat map in Figure 9B with a visual reference positioned above it in Figure 9A. With 90 mol% **(*S*)-1**, the mixture forms the expected (+)-**A**→(+)-**B**→(−)-**C** transitions as the mixture is cooled from the molecularly dissolved state **M**. However, at 80 mol% sergeant, the system remarkably exhibits a preferred helicity assigned to four different structures as it is cooled from 95 to 5 °C, proceeding through the sequence of **M**→(+)-**A**→(−)-**A**→(+)-**B**→(−)-**C**. At lower levels of **(*S*)-1** content, the system preferentially forms (−)-**A** over (+)-**A** within the expected temperature window depending on the water content. The elongation temperature of (+)-**A** (at high sergeant fractions) and (−)-**A** (at low sergeant fractions) consistently decreases as the sergeant fraction is decreased. The VT-UV absorption traces closely match the shape of the CD traces (Figures S27–S35). Thus, given the decreasing elongation temperature of (+)-**A**→(+)-**B** and (−)-**A**→(+)-**B** as the sergeant content is reduced from 90 to 10%, copolymerization is less thermodynamically favorable than the homopolymerization of **(*S*)-1** or ***iso*-1**. Nevertheless, the transitions (−)-**A**→(+)-**B** and (+)-**B**→(−)-**C** are sharp at all sergeant compositions, and the CD effect of chirality of (−)-**C** is strong even at low sergeant ratios.

It is clear that the subtle difference in molecular structure between ***n*-1** and ***iso*-1** leads to minute changes in thermodynamic stabilities that dramatically impact the polymer structure. The emergence of **(–)-A** in the S&S experiments with ***iso*-1** resemble earlier reports of the "abnormal" S&S effect observed in covalent polymers.[11,33-41] To the best of our knowledge, this is the first report of this effect in a helical supramolecular polymer. Interestingly, the distal substitution appears to only affect the copolymer structure of **A**, while the copolymers of **(*S*)-1** with both ***n*-1** and ***iso*-1** both form **(+)-B** and **(–)-C**. We propose that the tighter packing of the monomers in the polymers amplifies changes in steric repulsion between monomers, as the **A** copolymers do not incorporate water as a structural co-monomer. In contrast, due to the strong enthalpic release in the water-associated **(+)-B** and **(–)-C**, steric factors account for a smaller fraction of the stability of these polymers. The incorporation of ***iso*-1** imparts a different structure to the copolymers in state **A**, while the steric difference between ***iso*-1** and ***n*-1** is not sufficient to overcome the enthalpic stabilization in **(+)-B** and **(–)-C** to revert their helicities. This balance highlights the intriguing consequences of binding water to these supramolecular structures.

CONCLUSION

We have demonstrated the S&S effect across multiple helical states in the supramolecular copolymers of **(*S*)-1** with achiral co-monomers and water molecules. These copolymers show similar water-dependent helical structures as those observed for the **(*S*)-1** homopolymers. Computational techniques were essential for rationalizing the heterogeneous energy landscape evident in the S&S experiments with **(*S*)-1** with ***n*-1**. Despite the challenge of accurately quantifying the water concentration, we qualitatively explain the S&S results as a competition between the different helical states. This competitive nature can cause the sharpness and transition temperatures of the helical transitions to be dependent on the molar sergeant-soldier ratio. We also report an unprecedented example of the "abnormal" S&S effect in experiments using ***iso*-1** as the achiral soldier. The flip in preferred helical orientation of state **A** indicates that a delicate interplay between monomer structure and polymer morphology dominates supramolecular copolymerizations. Although the molecular structure of these co-assemblies remains elusive, it is evident that water has a profound impact on biasing their respective helicities. We hope that the phenomena and methodology outlined here will inspire the development of more structurally diverse monomers and copolymers, ultimately leading to control over the structure and function of dynamic macromolecular systems.

ASSOCIATED CONTENT

Experimental procedures, additional experiments, and raw data are provided in the Supporting Information. This material is available free of charge via the Internet at http://pubs.acs.org.

AUTHOR INFORMATION

Corresponding Author

* E-mail: nathan.van-zee@espci.psl.eu
e.w.meijer@tue.nl

Present Address

†École Normale Supérieure, Université PSL, UPMC Univ Paris 06, CNRS, Département de Chimie, PASTEUR, 24 rue Lhomond, 75005 Paris, France

Author Contributions

The manuscript was written through contributions of all authors. All authors have given approval to the final version of the manuscript.

ACKNOWLEDGMENT

This project received funding from the European Union's Horizon 2020 research and innovation program (no. 705701) and the NWO's TOP-PUNT grant (no. 10018944). The authors acknowledge the ICMS Animation Studio for their contribution of graphics. Part of this work was carried out on the Dutch national e-infrastructure with the support of SURF Cooperative.

REFERENCES

(1) Blackmond, D. G. The origin of biological homochirality. *Philos. Trans. R. Soc. B* **2011**, *366*, 2878-2884.

(2) Green, M. M.; Cheon, K. S.; Yang, S. Y.; Park, J. W.; Swansburg, S.; Liu, W. Chiral studies across the spectrum of polymer science. *Acc. Chem. Res.* **2001**, *34*, 672-680.

(3) Green, M. M.; Reidy, M. P.; Johnson, R. D.; Darling, G.; O'Leary, D. J.; Willson, G. Macromolecular stereochemistry: the out-of-proportion influence of optically active comonomers on the conformational characteristics of polyisocyanates. The sergeants and soldiers experiment. *J. Am. Chem. Soc.* **1989**, *111*, 6452-6454.

(4) Yashima, E.; Maeda, K.; Iida, H.; Furusho, Y.; Nagai, K. Helical polymers: synthesis, structures, and functions. *Chem. Rev.* **2009**, *109*, 6102-6211.

(5) Liu, M.; Zhang, L.; Wang, T. Supramolecular chirality in self-assembled systems. *Chem. Rev.* **2015**, *115*, 7304-7397.

(6) Yashima, E.; Ousaka, N.; Taura, D.; Shimomura, K.; Ikai, T.; Maeda, K. Supramolecular helical systems: helical assemblies of small molecules, foldamers, and polymers with chiral amplification and their functions. *Chem. Rev.* **2016**, *116*, 13752-13990.

(7) Bergueiro, J.; Freire, F.; Wendler, E. P.; Seco, J. M.; Quiñoá, E.; Riguera, R. The ON/OFF switching by metal ions of the "Sergeants and Soldiers" chiral amplification effect on helical poly(phenylacetylene)s. *Chem. Sci.* **2014**, *5*, 2170-2176.

(8) Arias, S.; Bergueiro, J.; Freire, F.; Quinoa, E.; Riguera, R. Chiral Nanostructures from Helical Copolymer-Metal Complexes: Tunable Cation-pi Interactions and Sergeants and Soldiers Effect. *Small* **2016**, *12*, 238-244.

(9) Nagata, Y.; Nishikawa, T.; Suginome, M. Solvent Effect on the Sergeants-and-Soldiers Effect Leading to Bidirectional Induction of Single-Handed Helical Sense of Poly(quinoxaline-2,3-diyl)s Copolymers in Aromatic Solvents. *ACS Macro Lett.* **2016**, *5*, 519-522.

(10) Zhao, B.; Deng, J.; Yang, W. Emulsion copolymerization of substituted acetylenes for constructing optically active helical polymer nanoparticles. Synergistic effects and helicity inversion. *J. Polym. Sci., Part A: Polym. Chem.* **2016**, *54*, 1679-1685.

(11) Wang, S.; Chen, J.; Feng, X.; Shi, G.; Zhang, J.; Wan, X. Conformation Shift Switches the Chiral Amplification of Helical

Copoly(phenylacetylene)s from Abnormal to Normal "Sergeants-and-Soldiers" Effect. *Macromolecules* **2017**, *50*, 4610-4615.

(12) Arias, S.; Rodriguez, R.; Quinoa, E.; Riguera, R.; Freire, F. Chiral Coalition in Helical Sense Enhancement of Copolymers: The Role of the Absolute Configuration of Comonomers. *J. Am. Chem. Soc.* **2018**, *140*, 667-674.

(13) Cobos, K.; Quinoa, E.; Riguera, R.; Freire, F. Chiral-to-Chiral Communication in Polymers: A Unique Approach To Control Both Helical Sense and Chirality at the Periphery. *J. Am. Chem. Soc.* **2018**, *140*, 12239-12246.

(14) Ikai, T.; Shimizu, S.; Awata, S.; Shinohara, K.-i. Chiral Amplification in π-Conjugated Helical Polymers with Circularly Polarized Luminescence. *Macromolecules* **2018**, *51*, 2328-2334.

(15) Yan, Z.; Cai, S.; Tan, J.; Zhang, J.; Yan, C.; Xu, T.; Wan, X. Induced Circular Dichroism of Isotactic Poly(2-vinylpyridine) with Diverse and Tunable "Sergeants-and-Soldiers" Type Chiral Amplification. *ACS Macro Lett.* **2019**, *8*, 789-794.

(16) Freire, F.; Cobos, K.; Rodriguez, R.; Quinoa, E.; Riguera, R. From Sergeants and Soldiers to Chiral Conflict Effects in Helical Polymers by Acting on the Conformational Composition of the Comonomers. *Angew. Chem. Int. Ed.* **2020**.

(17) Ikai, T.; Ishidate, R.; Inoue, K.; Kaygisiz, K.; Maeda, K.; Yashima, E. Chiral/Achiral Copolymers of Biphenylylacetylenes Bearing Various Substituents: Chiral Amplification through Copolymerization, Followed by Enhancement/Inversion and Memory of the Macromolecular Helicity. *Macromolecules* **2020**, *53*, 973-981.

(18) Kim, T.; Mori, T.; Aida, T.; Miyajima, D. Dynamic propeller conformation for the unprecedentedly high degree of chiral amplification of supramolecular helices. *Chem. Sci.* **2016**, *7*, 6689-6694.

(19) Das, A.; Vantomme, G.; Markvoort, A. J.; Ten Eikelder, H. M. M.; Garcia-Iglesias, M.; Palmans, A. R. A.; Meijer, E. W. Supramolecular copolymers: structure and composition revealed by theoretical modeling. *J. Am. Chem. Soc.* **2017**, *139*, 7036-7044.

(20) Leyendecker, M.; Meyer, N. C.; Thiele, C. M. Development of new supramolecular lyotropic liquid crystals and their application as alignment media for organic compounds. *Angew. Chem. Int. Ed.* **2017**, *56*, 11471-11474.

(21) Vela, S.; Berrocal, J. A.; Atienza, C.; Meijer, E. W.; Martin, N. Mesoscopic helical architectures via self-assembly of porphyrin-based discotic systems. *Chem. Commun.* **2017**, *53*, 4084-4087.

(22) Ghosh, G.; Paul, M.; Sakurai, T.; Matsuda, W.; Seki, S.; Ghosh, S. Supramolecular chirality issues in unorthodox naphthalene diimide gelators. *Chem. Eur. J.* **2018**, *24*, 1938-1946.

(23) Pal, D. S.; Kar, H.; Ghosh, S. Controllable supramolecular polymerization via a chain-growth mechanism. *Chem. Commun.* **2018**, *54*, 928-931.

(24) Dudek, M.; Machalska, E.; Oleszkiewicz, T.; Grzebelus, E.; Baranski, R.; Szczesniak, P.; Mlynarski, J.; Zajac, G.; Kaczor, A.; Baranska, M. Chiral Amplification in Nature: Studying Cell-Extracted Chiral Carotenoid Microcrystals via the Resonance Raman Optical Activity of Model Systems. *Angew. Chem. Int. Ed.* **2019**, *58*, 8383-8388.

(25) Greciano, E. E.; Calbo, J.; Buendia, J.; Cerda, J.; Arago, J.; Orti, E.; Sanchez, L. Decoding the Consequences of Increasing the Size of Self-Assembling Tricarboxamides on Chiral Amplification. *J. Am. Chem. Soc.* **2019**, *141*, 7463-7472.

(26) Valera, J. S.; Gomez, R.; Sanchez, L. Kinetic traps to activate stereomutation in supramolecular polymers. *Angew. Chem. Int. Ed.* **2019**, *58*, 510-514.

(27) Li, Y.; Hammoud, A.; Bouteiller, L.; Raynal, M. Emergence of Homochiral Benzene-1,3,5-tricarboxamide Helical Assemblies and Catalysts upon Addition of an Achiral Monomer. *J. Am. Chem. Soc.* **2020**, *142*, 5676-5688.

(28) Dorca, Y.; Naranjo, C.; Ghosh, G.; Gómez, R.; Fernández, G.; Sánchez, L. Unconventional Chiral Amplification in Luminescent Supramolecular Polymers Based on Trisbiphenylamine-tricarboxamides. *Org. Mater.* **2020**, *02*, 041-046.

(29) Yamada, T.; Nagata, Y.; Suginome, M. Non-hydrogen-bonding-based, solvent-dependent helix inversion between pure P-helix and pure M-helix in poly(quinoxaline-2,3-diyl)s bearing chiral side chains. *Chem. Commun.* **2010**, *46*, 4914-4916.

(30) Yamamoto, T.; Yamada, T.; Nagata, Y.; Suginome, M. High-molecular-weight polyquinoxaline-based helically chiral phosphine (PQXphos) as chirality-switchable, reusable, and highly enantioselective monodentate ligand in catalytic asymmetric hydrosilylation of styrenes. *J. Am. Chem. Soc.* **2010**, *132*, 7899-7901.

(31) Nagata, Y.; Yamada, T.; Adachi, T.; Akai, Y.; Yamamoto, T.; Suginome, M. Solvent-dependent switch of helical main-chain chirality in sergeants-and-soldiers-type poly(quinoxaline-2,3-diyl)s: effect of the position and structures of the "sergeant" chiral units on the screw-sense induction. *J. Am. Chem. Soc.* **2013**, *135*, 10104-10113.

(32) Nagata, Y.; Nishikawa, T.; Suginome, M.; Sato, S.; Sugiyama, M.; Porcar, L.; Martel, A.; Inoue, R.; Sato, N. Elucidating the Solvent Effect on the Switch of the Helicity of Poly(quinoxaline-2,3-diyl)s: A Conformational Analysis by Small-Angle Neutron Scattering. *J. Am. Chem. Soc.* **2018**, *140*, 2722-2726.

(33) Maeda, K.; Okamoto, Y. Synthesis and Conformational Characteristics of Poly(phenyl isocyanate)s Bearing an Optically Active Ester Group. *Macromolecules* **1999**, *32*, 974-980.

(34) Koe, J. R.; Fujiki, M.; Motonaga, M.; Nakashima, H. Cooperative Helical Order in Optically Active Poly(diarylsilylenes). *Macromolecules* **2001**, *34*, 1082-1089.

(35) Morino, K.; Maeda, K.; Okamoto, Y.; Yashima, E.; Sato, T. Temperature Dependence of Helical Structures of Poly(phenylacetylene) Derivatives Bearing an Optically Active Substituent. *Chem. Eur. J.* **2002**, *8*, 5112-5120.

(36) Tabei, J.; Shiotsuki, M.; Sato, T.; Sanda, F.; Masuda, T. Control of helix sense by composition of chiral-achiral copolymers of N-propargylbenzamides. *Chem. Eur. J.* **2005**, *11*, 3591-3598.

(37) Takei, F.; Onitsuka, K.; Takahashi, S.; Terao, K.; Sato, T. Control of Helical Structure in Random Copolymers of Chiral and Achiral Aryl Isocyanides Prepared with Palladium–Platinum μ-Ethynediyl Complexes. *Macromolecules* **2007**, *40*, 5245-5254.

(38) Sanada, Y.; Terao, K.; Sato, T. Double screw-sense inversions of helical chiral-achiral random copolymers of fluorene derivatives in phase separating solutions. *Polym. J.* **2011**, *43*, 832-837.

(39) Nagata, Y.; Nishikawa, T.; Suginome, M. Exerting control over the helical chirality in the main chain of sergeants-and-soldiers-type poly(quinoxaline-2,3-diyl)s by changing from random to block copolymerization protocols. *J. Am. Chem. Soc.* **2015**, *137*, 4070-4073.

(40) Nagata, Y.; Nishikawa, T.; Suginome, M. Abnormal sergeants-and-soldiers effects of poly(quinoxaline-2,3-diyl)s enabling discrimination of one-carbon homologous n-alkanes through a highly sensitive solvent-dependent helix inversion. *Chem. Commun.* **2018**, *54*, 6867-6870.

(41) Wada, Y.; Shinohara, K. I.; Asakawa, H.; Matsui, S.; Taima, T.; Ikai, T. One-Step Synthesis of One-Dimensional Supramolecular Assemblies Composed of Helical Macromolecular Building Blocks. *J. Am. Chem. Soc.* **2019**, *141*, 13995-14002.

(42) Aratsu, K.; Takeya, R.; Pauw, B. R.; Hollamby, M. J.; Kitamoto, Y.; Shimizu, N.; Takagi, H.; Haruki, R.; Adachi, S. I.; Yagai, S. Supramolecular copolymerization driven by integrative self-sorting of hydrogen-bonded rosettes. *Nat. Commun.* **2020**, *11*, 1623.

(43) Sorrenti, A.; Leira-Iglesias, J.; Markvoort, A. J.; de Greef, T. F. A.; Hermans, T. M. Non-equilibrium supramolecular polymerization. *Chem. Soc. Rev.* **2017**, *46*, 5476-5490.

(44) Adelizzi, B.; Van Zee, N. J.; de Windt, L. N. J.; Palmans, A. R. A.; Meijer, E. W. Future of Supramolecular Copolymers Unveiled by Reflecting on Covalent Copolymerization. *J. Am. Chem. Soc.* **2019**, *141*, 6110-6121.

(45) Van Zee, N. J.; Adelizzi, B.; Mabesoone, M. F. J.; Meng, X.; Aloi, A.; Zha, R. H.; Lutz, M.; Filot, I. A. W.; Palmans, A. R. A.; Meijer, E. W. Potential enthalpic energy of water in oils exploited to control supramolecular structure. *Nature* **2018**, *558*, 100-103.

(46) Markvoort, A. J.; ten Eikelder, H. M.; Hilbers, P. A.; de Greef, T. F.; Meijer, E. W. Theoretical models of nonlinear effects in two-component cooperative supramolecular copolymerizations. *Nat Commun* **2011**, *2*, 509.

(47) Smulders, M. M.; Filot, I. A.; Leenders, J. M.; van der Schoot, P.; Palmans, A. R.; Schenning, A. P.; Meijer, E. W. Tuning the extent of chiral amplification by temperature in a dynamic supramolecular polymer. *J. Am. Chem. Soc.* **2010**, *132*, 611-619.

(48) Ten Eikelder, H. M. M.; Adelizzi, B.; Palmans, A. R. A.; Markvoort, A. J. Equilibrium Model for Supramolecular Copolymerizations. *J. Phys. Chem. B* **2019**, *123*, 6627-6642.

(49) Das, A.; Vantomme, G.; Markvoort, A. J.; Ten Eikelder, H. M. M.; Garcia-Iglesias, M.; Palmans, A. R. A.; Meijer, E. W. Supramolecular Copolymers: Structure and Composition Revealed by Theoretical Modeling. *J. Am. Chem. Soc.* **2017**, *139*, 7036-7044.

(50) Adelizzi, B.; Aloi, A.; Markvoort, A. J.; Ten Eikelder, H. M. M.; Voets, I. K.; Palmans, A. R. A.; Meijer, E. W. Supramolecular Block Copolymers under Thermodynamic Control. *J. Am. Chem. Soc.* **2018**, *140*, 7168-7175.

(51) Berrocal, J. A.; Mabesoone, M. F. J.; Garcia Iglesias, M.; Huizinga, A.; Meijer, E. W.; Palmans, A. R. A. Selenoamides modulate dipole-dipole interactions in hydrogen bonded supramolecular polymers of 1,3,5-substituted benzenes. *Chem. Commun.* **2019**, 55, 14906-14909.

(52) de Windt, L. N. J.; Kulkarni, C.; Ten Eikelder, H. M. M.; Markvoort, A. J.; Meijer, E. W.; Palmans, A. R. A. Detailed Approach to Investigate Thermodynamically Controlled Supramolecular Copolymerizations. *Macromolecules* **2019**, 52, 7430-7438.

(53) Mabesoone, M. F. J.; Meijer, E. W. Counterintuitive consequences of competitive pathways in supramolecular polymerizations. *J. Polym. Sci.* **2020**, *58*, 25-29.

.

TOC: